JOURNAL OF CHEMICAL & ENGINEERING DATA

ARTICLE

pubs.acs.org/jced

Differential Scanning Calorimetry Study on Thermal Denaturation of Human Carbonic Anhydrase II

Mojtaba Amani,[*,†] Reza Khodarahmi,[‡] Sirous Ghobadi,[§] Masomeh Mehrabi,[‡,§] Boris I. Kurganov,[⊥] and Ali Akbar Moosavi-Movahedi[∥]

[†]Faculty of Medicine, Ardabil University of Medical Sciences, Ardabil, Iran

[‡]Department of Pharmacognosy and Biotechnology, Faculty of Pharmacy (and Medical Biology Research Center), Kermanshah University of Medical Sciences, Kermanshah, Iran

[§]Department of Biology, Faculty of Science, Razi University, Kermanshah, Iran

[⊥]Bakh Institute of Biochemistry, Russian Academy of Sciences, Leninski prospect 33, Moscow, Russia

[∥]Institute of Biochemistry and Biophysics, University of Tehran, Tehran, Iran

ABSTRACT: The thermal unfolding of human carbonic anhydrase II (HCAII) has been studied by circular dichroism, UV−vis spectrophotometry, and differential scanning calorimetry (DSC). Coincidence of aggregation and tertiary structure disruption as well as fitting of DSC data showed that a two-state model can properly explain thermal unfolding of HCAII. According to this model, the average values of T^* (the temperature at which $k = 1/60\ s^{-1}$), ΔH (enthalpy), and ΔE_a (activation energy) are equal to 335.8 K, 698.6 kJ·mol^{-1}, and 529.0 kJ·mol^{-1}, respectively.

INTRODUCTION

Protein folding and unfolding are one of the research fields of interest of scientists working in different areas. An investigation on this topic will pave the fundamental basis for understanding the protein structure−stability relationship and the factors affecting them. In the field of biotechnology, this knowledge can be applied to increase stability of biocatalysts and carrying out enzymatic process at higher temperatures. In medicine there are several diseases caused by protein misfolding. For example, marble brain syndrome (MBS) disease, known also as carbonic anhydrase II deficiency syndrome (CADS), can manifest in carriers of point mutations, His107Tyr substitution, in the human carbonic anhydrase II (HCAII) gene. Almstedt et al. demonstrated that this mutation has a remarkably destabilizing effect.[1]

For the first time, carbonic anhydrase (CA; carbonate hydrolyase, EC 4.2.1.1) was isolated by Margaria from ox blood in 1932.[2] CA is a zinc metalloenzyme catalyzing both phases of the reversible reaction $H_2CO_3 \leftrightarrows CO_2 + H_2O$; thus, it is physiologically important in the formation of CO_2 from bicarbonate in the lung. The various types of CA have been isolated from animal and plant cells and have been also found in some strains of the bacterial genus *Neisseria*. It has been shown that there exist five evolutionarily unrelated CA families named as α- (found in animals), β- (mostly found in higher plants), γ-CA (produced by the methanogenic archaebacterium, *Methunosarcina thermoghila*, when grown on acetate), δ-CAs (present in some marine diatoms), and ζ-CA (found in marine diatoms which contain Cd instead of Zn in their active site).[3] There are no significant sequence homologies between different CA families. In higher vertebrates, including humans, 16 different CA isozymes or CA-related proteins (CARP) have been described.[3,4]

In human, seven α-CA isoenzymes have been identified differing in their location in tissues and cells, catalytic efficiency, inhibitor binding, and gene sequence. Four types of them are cytosolic; HCAI, II, III, and VII. The isoenzyme with highest turnover rate, HCAII, is traditionally purified from red blood cells. HCAII plays an important role in bone, kidney, and brain functions so the HCAII deficiency may cause syndromes like osteoporosis, renal tubular acidosis, and cerebral calcification.[5,6]

X-ray crystallography studies showed that the active site forms a cavity almost in the center of the molecule. A zinc ion is located near the bottom of the cavity. Zinc ligands to three nitrogen atoms from His-94, His-96, and His-119 are in a tetrahedral geometry, with an H_2O or OH^-.[1,7]

Lavecchia and Zugaro carried out an experimental study on the thermal behavior of erythrocyte CA to estimate the thermodynamic parameters of the enzyme. They also studied the effects of thermal denaturation on the catalytic properties of the enzyme. According to their results, below 333 K the enzyme is very stable, whereas between (333 and 338) K a drastic decrease in the biological activity is observed.[8] They reported that the loss of HCAII activity is an irreversible process, while HCAII showed a reversible thermal unfolding using UV−vis spectrophotometry. They reported T_m, van't Hoff enthalpy (ΔH_{vH}), and ΔG at 298 K equal to 335.6 K, 1075 kJ·mol^{-1}, and 83.7 kJ·mol^{-1}, respectively. They described discrepancy in the reversibility seen in structural changes and thermal inactivation as the former reflects major structural changes, whereas the latter is related to local modifications of the active site region which cannot be properly rearrange upon cooling. In the other report by Matulis et al., represented thermograms of bovine CAII unfoldings in several buffers of

Special Issue: John M. Prausnitz Festschrift

Received: October 24, 2010
Accepted: January 18, 2011
Published: February 10, 2011

varying pH, inhibitor, and ligand concentration using Thermo-Fluor and differential scanning calorimetry (DSC).[9] They reported the T_m and ΔH_{vH} for bovine CAII equal to 337 K and 795 kJ·mol^{-1}, respectively. According to their study, the calorimetric and van't Hoff enthalpies are similar. On the basis of a two-state reversible unfolding model, the data were analyzed, while they stated that thermal unfolding of CAII is an irreversibility process.

The thermal unfolding transitions of apo- and holo-HCAII have been studied by Avvaru et al., using DSC and fitting the data to a two-state reversible unfolding model.[10] They observed a dominant endothermic peak for both holo- and apo-HCAII. The holo enzyme showed a peak at (332 ± 0.5) K with a peak area of 1171.52 kJ·mol^{-1}, while those of the apo-HCAII were 324 K and 1046 kJ·mol^{-1}, respectively. They showed that the T_m values obtained from DSC were 2 K lower than the circular dichroism (CD) values for both apo and holo-HCAII. They explained that this discrepancy can be a consequence of different protein concentration and buffers.[10] We believe that this effect may arise from the irreversibility of HCAII denaturation and rate dependency of the T_m values.

By studying the 8-(phenylamino)-1-naphthalene sulfonic acid (ANS) binding to thermally denatured HCAII, Kundu and Guptasarma showed that ANS binding can inhibit the HCAII aggregation; they conclude that the main reason for irreversibility of HCAII thermal denaturation is due to hydrophobic surfaces in denatured protein which can be prevented by hydrophobic dye, ANS.[11]

In previous studies the thermal unfolding of CAII was treated as a reversible unfolding process, while in all of them there were some signs of irreversibility. The main aims of this study were to gain information about the kinetic parameters that control the unfolding of the HCAII and to present a model for this process. Since differential scanning calorimetry (DSC) is the most useful technique for the determination of thermodynamic parameters, for these can be determined directly by it, the present work mainly based on DSC experiments while other techniques are also been used.

MATERIALS AND METHODS

Carbonic Anhydrase Purification and Protein Detection. Human CAII isoenzyme was purified from red blood cells according to Nyman's method,[12] with some minor modifications. The concentration of CA was determined by absorbance at 280 nm with an extinction coefficient (ε_{280}) of 5.7·10^4 mol^{-1}·cm^{-1}.[13]

Enzyme Assay and Its Thermal Inactivation. The enzymatic activity of HCAII solution was determined based on 4-nitrophenyl acetate (pNPAc) esterase activity of the enzyme according to Pocker and Stone.[14] For the thermal inactivation of HCAII, the enzyme was incubated in sealed vials at various temperatures of (310 to 343 K). At each 300 s interval an aliquot of enzyme solution was removed from the incubated sample and cooled immediately to 298 K by a thermostatic water circulator. The thermal inactivation of HCAII was determined by comparing the initial rates of 4-nitrophenyl acetate hydrolysis of incubated HCAII and the native one at 298 K.

Circular Dichroism and Aggregation Measuring. CD spectra were recorded in a J-810 spectropolarimeter (Jasco Corporation, Tokyo, Japan) using a cuvette path length of 0.2 cm for far-UV and 1 cm for near-UV CD. The temperature was controlled with a Peltier type thermoelectric cell holder (Jasco PTC-423S). Thermal stability experiments were performed between (298 and 348) K with a constant heating rate of 1/60 K per second and scan rate of 300 nm·h^{-1}. Mean residue ellipticity (MRE) values were followed at 222 nm for far-UV CD and 280 nm for near-UV CD. Dynode voltages were measured at 280 nm, to detect the aggregation of HCAII upon heating.[15]

Differential Scanning Calorimetry. The thermal denaturation of HCAII was studied by Nano-DSCII Setaram (Setaram, France). The protein unfolding was studied in the temperature region of (298 to 388) K at various scanning rates ranging from (15 to 120) K·h^{-1}. To avoid any possible blobbing, all solutions were degassed, and experiments were carried out under 2 kPa pressure. The volume of sample and reference cells was 342·10^{-9} m^3, and the concentrations of protein solutions were (0.5, 1, 2.5, and 5) kg·m^{-3}.

Analysis of DSC Data. It is believed that the reason for irreversibility of protein denaturation is the presence of a step where protein undergoes irreversible alterations. This prospective can be shown in simple Lumry−Eyring model. In this model, reversible unfolding of protein is followed by an irreversible process as:

$$N \underset{k_{-1}}{\overset{k_1}{\rightleftarrows}} U \xrightarrow{k_2} F \qquad \text{(Model 1)}$$

where N, U, and F are the native, unfolded, and final denatured states of protein, respectively. k_1, k_{-1}, and k_2 are rate constants for each reaction.

The excess molar heat capacity (C_p^{E}) dependence on temperature for the formal Lumry−Eyring model with a fast equilibrating first step was calculated as:[16]

$$C_p^{E} = \left[\frac{K\Delta H_u}{\{K+1\}^2}\left(\frac{k_2}{\nu}+\frac{\Delta H_u}{RT^2}\right)+\Delta H_i\frac{1}{\nu}\frac{k_2K}{K+1}\right] \exp\left(-\frac{1}{\nu}\int_{T0}^{T}\frac{k_2K}{K+1}dT\right) \qquad (1)$$

where ΔH_u, ΔH_i, K, and k_2 are the changes in the enthalpy for the first step, changes in the enthalpy for the second step, equilibrium constant, and rate constant for the second step, respectively. K and k are temperature-dependent parameters given by the relations:

$$K = \exp\left(-\frac{\Delta H_u}{R}\left(\frac{1}{T}-\frac{1}{T_{1/2}}\right)\right) \qquad (2)$$

$$k = \exp\left(-\frac{E}{R}\left(\frac{1}{T}-\frac{1}{T^*}\right)\right) \qquad (3)$$

$T_{1/2}$ is the temperature at which K = 1, and T^* is the temperature at which k = 1/60 s^{-1}.

The Lumry−Eyring model can be written in different forms. For example, if k_2 is sufficiently high relative to k_1, the N transforms to F without significant accumulation of U state, so in this situation, the Lumry−Eyring model can be reduced to a two-state (also named as one step) model:

$$N \xrightarrow{k} F \qquad \text{(Model 2)}$$

dx.doi.org/10.1021/je101087j |J. Chem. Eng. Data 2011, 56, 1158–1162

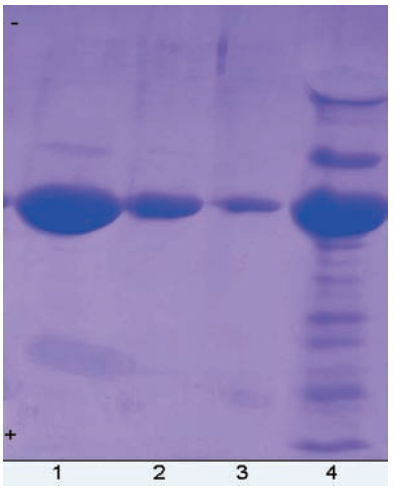

Figure 1. SDS-PAGE pattern of the purified (lanes 1 to 3) and commercial (lane 4) CA. Electrophoresis was performed on a 0.10 mass fraction slab gel.

The dependence of heat capacity on temperature for two-state model has been proposed as:[17]

$$C_p^{\mathrm{E}} = \frac{1}{\nu}\,\Delta H\,\exp\left(\frac{E_a}{R}\left(\frac{1}{T^*}-\frac{1}{T}\right)\right)\exp\left[-\frac{1}{\nu}\int_{T0}^{T}\exp\left(\frac{E_a}{R}\left(\frac{1}{T^*}-\frac{1}{T}\right)\right)\right] \quad (4)$$

In which C_p^{E}, ΔH, E_a, T, and T^* are the excess heat capacity, enthalpy of denaturation, activation energy, and temperature at which $k = 1/60\ \mathrm{s}^{-1}$, respectively.

Using the EXCELSOLVER program, the experimental data were fitted to the two-step model (eq 3).

The qualities of fittings were judged by R (correlation coefficient) values which are calculated as:

$$R = \sqrt{1 - \sum_{i=1}^{n}(y_i - y_i^{\mathrm{calc}})^2 \Big/ \sum_{i=1}^{n}(y_i - y_i^{m})^2} \quad (5)$$

where y_i and y_i^{calc} are the experimental and calculated values of C_p^{E}, y_i^{m} is the mean value of experimental C_p^{E}, and n is the number of temperatures at which C_p^{E} has been measured.[18]

RESULTS

Purification of HCAII. The enzyme identity and purity were tested by sodium dodecyl sulfate-polyacrylamide gel electrophoresis (SDS-PAGE) and by comparing with commercial HCAII enzyme. The SDS-PAGE analysis is shown in Figure 1 which clearly indicates the reasonable purity of the isolated enzyme. The densitometry of bands indicates that the mass fraction of purified HCAII is more than 0.95.

Thermal Inactivation of HCAII. HCAII incubated at different temperatures for 300 s and then cooled to 298 K. The activity of samples is completely reversible up to 318 K, while above this temperature HCAII cannot regain complete activity by cooling (Figure 2).

Thermal Denaturation Study Using UV−vis Spectrophotometry. The reversibility of HCAII thermal denaturation was checked using UV−vis spectrophotometer by following changes

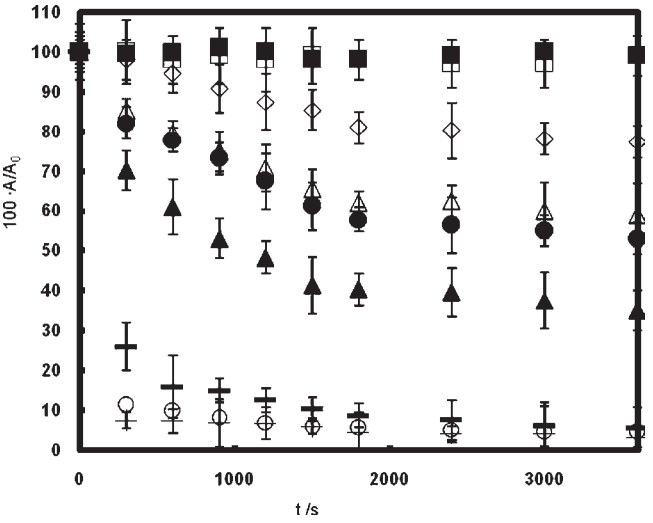

Figure 2. Fraction of residual activity A/A_0 of HCAII incubated at ■, 310 K; □, 313 K; ◇, 318 K; △, 322 K; ●, 325 K; ▲, 328 K; —, 331 K; ○, 334 K; and +, 338 K as a function of incubation time. Data are the mean values of three independent experiments.

in (278 and 350) nm at different temperatures. Absorbances at (278 and 350) nm increase above 323 K coincidently which indicate that at least some parts of changes seen at 278 nm may arise from aggregation of HCAII. The presence of aggregation and different UV−vis profiles of the native and denatured HCAII (heated up to 338 K) indicate that thermal denaturation of HCAII is an irreversible process (data not shown).

Circular Dichroism Experiments. Thermal denaturation of HCAII was further investigated by CD. Thermal denaturation of HCAII was followed by molar ellipticity at 222 nm for far-UV CD and at 280 nm for near-UV CD. The change in molar ellipticity at 222 nm shows two steps (Figure 3a). First, the negative molar ellipticity of HCAII increases in the range of (323 to 330) K and then decreases in the negative molar ellipticity in temperatures higher than 330 K, while molar ellipticity at 280 nm shows just one increasing phase, starting at 329 K. The increase in dynode voltage and changes in molar ellipticity at 280 nm occur simultaneously (Figure 3a and b). The coincidence of these events mean that HCAII undergoes the aggregation process as its tertiary structure disrupts. It is worthy noting that decreases in both parameters seen above 333 K may arise from precipitation of the aggregated protein.

Differential Scanning Calorimetry. Differential scanning calorimetry (DSC) study shows a major transition without any distinct peak for aggregation. The DSC profile is not replicable in the heated HCAII (1 to 2) K above T_m (Figure 4). To obtain the appropriate model and kinetic parameters of irreversible denaturation of HCAII, a series of DSC experiments were performed at different scanning rates and various enzyme concentrations. The transition shows a scan rate-dependent T_m, while the peak area is independent of scan rate. The dependency of T_m to heating scanning rate indicates that the thermal denaturation of HCAII is kinetically controlled. T_m and ΔH are independent of HCAII concentration in the range of (0.5 to 5) $\mathrm{kg\cdot m^{-3}}$. Regardless of scan rate, the increase of C_p^{E} starts up at 325 K, but the ending point is scan rate dependent, and it decreases as the scan rate decreases.

Analysis of DSC Data. The DSC data were fitted to eq 4. Fitting to a two-state model gives reliable results, and the variations in fitting parameters at varying scan rates are not as much. Figure 5 shows the

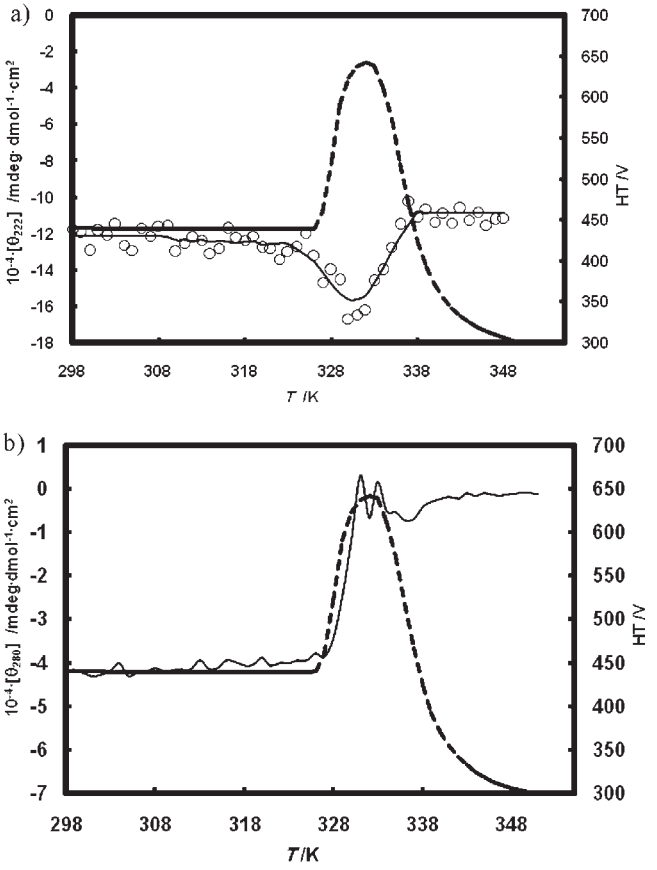

Figure 3. Thermal unfolding of HCAII in Tris buffer (pH 7.8), followed by MRE $[\theta_{280}]$ (left axis and solid line) at 222 nm (a) and 280 nm (b) as a function of temperature T. In both plots the dashed line on right axis shows the dynode voltage HT at 280 nm as an indicator of aggregation respect to temperature. Circles in plot 3a show the experimental values of MRE, and the continuous line is the smoothed data. In all CD experiments, the heating rate was 60 K·h^{-1}. In far- and near-UV CD experiments, HCAII concentrations were 0.32 kg·m^{-3} and 3.5 kg·m^{-3}, respectively.

fitted DSC profile to eq 4 as well as fitting parameters to a two-state model are presented in Table 1.

DISCUSSION

In the thermodynamics aspect, in spite of irreversible thermal denaturation of HCAII, in previous investigations the HCAII unfolding has been treated as a reversible process. In some studies, curves were fitted to an equilibrium two-state unfolding model to obtain van't Hoff enthalpies. The HCAII were purified (Figure 1), and the irreversibility of HCAII was checked by regaining the activity of thermally denatured HCAII upon cooling to 298 K. The result shows that the thermal unfolding of HCAII is an irreversible process in agreement with previous studies (Figure 2).

For more details, the thermal unfolding of HCAII was followed by CD. As it is seen in Figure 3a, the molar ellipticity of HCAII upon thermal denaturation changes in two steps: (1) increasing the negative molar ellipticity of HCAII in the range of (323 to 330) K and (2) decreasing the molar ellipticity of HCAII at temperatures above 330 K. Albeit the decrease in the negative molar ellipticity of HCAII upon unfolding seems to be an odd process, but indeed such a decrease has been shown in some proteins, for example, ceruloplasmin.[19] This phenomenon indicates that there is some

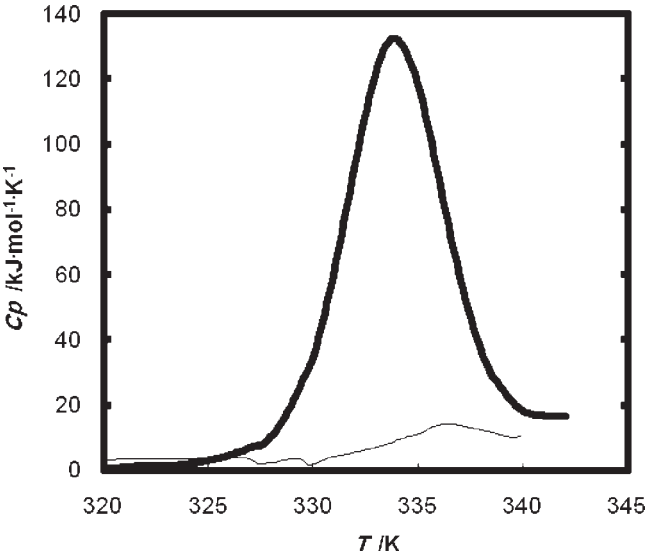

Figure 4. Heat capacity C_p of the native (thick line) and rescan of human CA heated (1 to 2) K above T_m (thin line) as a function of temperature T.

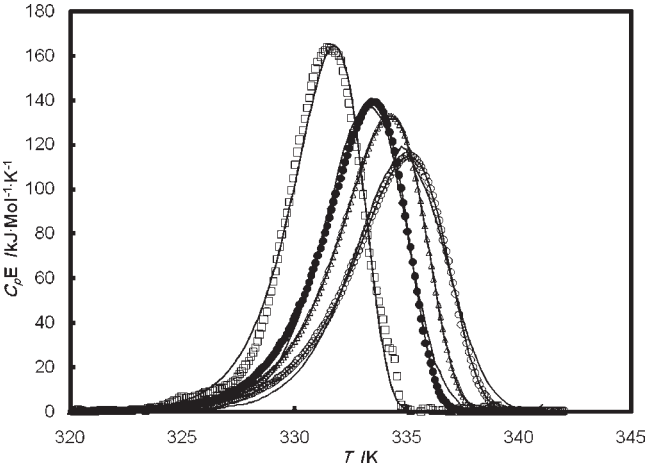

Figure 5. Experimental (symbols) and fitted values to a two-state model (continuous line) of excess heat capacity C_p^E of human CA as a function of temperature T at scanning rates of □, 7.5 K·h^{-1}; ●, 30 K·h^{-1}; △, 60 K·h^{-1}; and ○, 120 K·h^{-1}.

residual structure in the thermally denatured form of protein. The second step can be due to the accumulation and precipitation of the aggregated form of HCAII. To validate this possibility the dynode voltage of CD data was investigated, since increasing the dynode voltage is a sign of aggregation.[15] As can be seen in Figure 3a and b, the increase of dynode voltage and changes in the negative molar ellipticity of thermal denaturation of HCAII occurred almost simultaneously. These results show that thermal denaturation of HCAII is an irreversible process, and it goes to the aggregated form as it unfolds. This means that the unfolded state of HCAII cannot be accumulated, and it immediately goes to the final state of Lumry—Eyring model. Fitting the DSC data to a two-state Model 2model II is shown in Figure 5. Considering all results together, we conclude that HCAII undergoes a two-state irreversible thermal denaturation.

By Lyubarev and Kurganov's opinion, a two-step model has gained general acceptance and gives best fitting data at different

dx.doi.org/10.1021/je101087j |J. Chem. Eng. Data 2011, 56, 1158–1162

Table 1. Enthalpy (ΔH), Activation Energy (E_a), and the Temperature at Which the Constant Rate Equals 1/60 s^{-1} (T^*) Obtained at Different Scanning Rates by Fitting of DSC Profile to eq 4

scan rate	ΔH	E_a	T^*	
$K \cdot h^{-1}$	$kJ \cdot mol^{-1}$	$kJ \cdot mol^{-1}$	K	R
7.5	720.51	600.29	335.71	> 0.99
15	742.25	541.48	336.86	> 0.99
30	684.45	535.32	335.77	> 0.99
60	699.16	500.63	335.51	> 0.99
120	646.48	467.45	335.19	> 0.99
mean value	698.57	529.03	335.81	
SD	36.41	49.68	0.63	

scan rates.[16] Also they expressed several examples of DSC data fitted to eq 4 in which the optimal values of parameters are different, so they suggested studying DSC experiments in combination with other techniques to provide sufficient information about protein thermal denaturation.[16]

Our study also shows that the starting point of thermal denaturation of HCAII is 325 K by means of DSC and near-CD, while the secondary structure disrupts at 323 K. Far-UV CD measures the chirality of the peptide bond and, specially, reports change in secondary structure, while near-UV CD probes the chiral environment of aromatic residues, making it an excellent probe of tertiary structure. DSC is used to analyze more deeply the overall denaturation process,[20] and it measures the heat (enthalpy) required to break the noncovalent interactions that stabilizes the native conformation during thermal unfolding.[21] Since both near-UV CD and DSC monitor the overall structural changes, the study of the DSC in accompanying with the near-CD may give better results relative to the far-UV CD.

■ CONCLUSION

Thermal denaturation of HCAII follows a two-state irreversible thermal denaturation with the mean values of T^*, ΔH, and ΔE_a as (335.8 ± 0.6) K, (698.6 ± 36.4) $kJ \cdot mol^{-1}$, and (529.0 ± 49.7) $kJ \cdot mol^{-1}$, respectively. The aggregation of HCAII does not show a distinct DSC peak. Although the secondary structure disruption precedes the aggregation, tertiary structure disruption coincides with aggregation. This means that aggregation of HCAII is a very rapid process based on the Lumry−Eyring model where $k_2 \gg k_1$ and $k_2 \gg k_{-1}$ (see Model 1model 1).

■ AUTHOR INFORMATION

Corresponding Author

*E-mail: m.amani@arums.ac.ir. Tel.: +98451-5512788. Fax: +98451-5510057.

Funding Sources

The support of University of Tehran, Ardabil University of Medical Sciences, Razi University, Kermanshah University of Medical Sciences, and Iran National Science Foundation (INSF) is acknowledged.

■ REFERENCES

(1) Almstedt, K.; Lundqvist, M.; Carlsson, J.; Karlsson, M.; Persson, B.; Jonsson, B. H.; Carlsson, U.; Hammarstrom, P. Unfolding a folding disease: folding, misfolding and aggregation of the marble brain syndrome-associated mutant H107Y of human carbonic anhydrase II. *J. Mol. Biol.* **2004**, *342*, 619–633.

(2) Meldrum, N. U.; Roughton, F. J. Carbonic anhydrase. Its preparation and properties. *J. Physiol.* **1933**, *80*, 113–142.

(3) Hewett-Emmett, D.; Tashian, R. E. Functional diversity, conservation, and convergence in the evolution of the alpha-, beta-, and gamma-carbonic anhydrase gene families. *Mol. Phylogenet. Evol.* **1996**, *5*, 50–77.

(4) Supuran, C. T.; Di Fiore, A.; Alterio, V.; Monti, S. M.; De Simone, G. Recent Advances in Structural Studies of the Carbonic Anhydrase Family: The Crystal Structure of Human CA IX and CA XIII. *Curr. Pharm. Des.* **2010**, *16*, 3246–3254.

(5) Sly, W. S.; Hewett-Emmett, D.; Whyte, M. P.; Yu, Y. S.; Tashian, R. E. Carbonic anhydrase II deficiency identified as the primary defect in the autosomal recessive syndrome of osteopetrosis with renal tubular acidosis and cerebral calcification. *Proc. Natl. Acad. Sci. U.S.A.* **1983**, *80*, 2752–2756.

(6) Sly, W. S.; Hu, P. Y. Human carbonic anhydrases and carbonic anhydrase deficiencies. *Annu. Rev. Biochem.* **1995**, *64*, 375–401.

(7) Stams, T.; Christianson, D. W. X-ray crystallographic studies of mammalian carbonic anhydrase isozymes. *EXS* **2000**, 159–174.

(8) Lavecchia, R.; Zugaro, M. Thermal denaturation of erythrocyte carbonic anhydrase. *FEBS Lett.* **1991**, *292*, 162–164.

(9) Matulis, D.; Kranz, J. K.; Salemme, F. R.; Todd, M. J. Thermodynamic stability of carbonic anhydrase: measurements of binding affinity and stoichiometry using ThermoFluor. *Biochemistry* **2005**, *44*, 5258–5266.

(10) Avvaru, B. S.; Busby, S. A.; Chalmers, M. J.; Griffin, P. R. Venkatakrishnan, B.; Agbandje-McKenna, M.; Silverman, D. N.; McKenna, R. Apo-human carbonic anhydrase II revisited: implications of the loss of a metal in protein structure, stability, and solvent network. *Biochemistry* **2009**, *48*, 7365–7372.

(11) Kundu, B.; Guptasarma, P. Hydrophobic dye inhibits aggregation of molten carbonic anhydrase during thermal unfolding and refolding. *Proteins* **1999**, *37*, 321–324.

(12) Nyman, P. O. Purification and properties of carbonic anhydrase from human erythrocytes. *Biochim. Biophys. Acta* **1961**, *52*, 1–12.

(13) Yazdanparast, R.; Khodarahmi, R.; Soori, E. Comparative studies of the artificial chaperone-assisted refolding of thermally denatured bovine carbonic anhydrase using different capturing ionic detergents and beta-cyclodextrin. *Arch. Biochem. Biophys.* **2005**, *437*, 178–185.

(14) Pocker, Y.; Stone, J. T. The catalytic versatility of erythrocyte carbonic anhydrase. 3. Kinetic studies of the enzyme-catalyzed hydrolysis of p-nitrophenyl acetate. *Biochemistry* **1967**, *6*, 668–678.

(15) Benjwal, S.; Verma, S.; Rohm, K. H.; Gursky, O. Monitoring protein aggregation during thermal unfolding in circular dichroism experiments. *Protein Sci.* **2006**, *15*, 635–639.

(16) Lyubarev, A. E.; Kurganov, B. I. Study of Irreversible Thermal Denaturation of Proteins by Differential Scanning Calorimetry. In *Methods in protein structure and stability analysis*, part C: Conformational stability, size, shape and surface of protein molecules; Uversky, V. N., Ed.; Nova Publishers: New York, 2007; pp 109−146.

(17) Lyubarev, A. E.; Kurganov, B. I.; Burlakova, A. A.; Orlov, V. N. Irreversible thermal denaturation of uridine phosphorylase from Escherichia coli K-12. *Biophys. Chem.* **1998**, *70*, 247–257.

(18) Milardi, D.; Rosa, C. L.; Grasso, D.; Guzzi, R.; Sportelli, L.; Fini, C. Thermodynamics and kinetics of the thermal unfolding of plastocyanin. *Eur. Biophys. J.* **1998**, *27*, 273–282.

(19) Sedlak, E.; Zoldak, G.; Wittung-Stafshede, P. Role of copper in thermal stability of human ceruloplasmin. *Biophys. J.* **2008**, *94*, 1384–1391.

(20) Rezaei, H.; Choiset, Y.; Eghiaian, F.; Treguer, E.; Mentre, P.; Debey, P.; Grosclaude, J.; Haertle, T. Amyloidogenic unfolding intermediates differentiate sheep prion protein variants. *J. Mol. Biol.* **2002**, *322*, 799–814.

(21) Ferguson, N.; Schartau, P. J.; Sharpe, T. D.; Sato, S.; Fersht, A. R. One-state downhill versus conventional protein folding. *J. Mol. Biol.* **2004**, *344*, 295–301.